13th International Symposium on Particle Image Velocimetry – ISPIV 2019
Munich, Germany, July 22-24, 2019

Study of Upstream Travelling Waves in Transonic Buffet

A. D'Aguanno[1]*, F.F.J. Schrijer[1], B.W. van Oudheusden[1]

[1] Delft University of Technology, Faculty of Aerospace Engineering, Aerodynamics Department, Kluyverweg 2, 2629HS, Delft, The Netherlands

* A.Daguanno@tudelft.nl

Abstract

This paper investigates the appearance, propagation and orientation of upstream travelling waves (UTWs) in transonic buffet. Their role has been studied experimentally on a supercritical airfoil (OAT15A) in the transonic-supersonic wind tunnel of TU Delft at Mach number of 0.7, and an angle of attack of 3.5. In the experiments Background Oriented Schlieren (BOS) and Particle Image Velocimetry (PIV) have been used, to observe the suction side of the airfoil in a streamwise-spanwise oriented plane. The experiments detected the frequency and propagation velocity of the UTWs, which have been confirmed to behave as acoustic waves that therefore travel at the speed of sound relative to the flow. The particular set-up configuration used confirmed the two-dimensionality of the velocity field and of the shock wave but showed that the UTWs propagate in the plane of measurement with a non-zero orientation.

1 Introduction

Transonic buffet is a phenomenon which consists in the oscillation of a shock wave on the suction side of a wing for a certain range of *Ma,* α and *Re* values. The first studies on transonic buffet were undertaken by Hilton and Fowler (1952). However, despite being widely studied in the past 30 years, the mechanism on which buffet is based has not been completely understood yet. The shock buffet oscillation was found to be sustained by a feedback mechanism, as introduced by Lee (1990), who described the presence of upstream travelling waves (UTWs) and of downstream travelling waves (DTWs) as responsible for sustaining the shock oscillation as shown in Fig. 1. Therefore, the shock oscillation is sustained by an exchange of energy between the shock itself and the UTWs, which, depending on the phase, force the shock to move upstream or downstream. This model has been updated by Garnier and Deck (2010), who considered the UTWs to be able to travel along the pressure side too. However, the nature of the DTWs and of the UTWs has not been fully understood. Lee (1990) and Jacquin et al. (2009) described DTWs as being created at the shock foot, but it remains unclear whether they are created there or in the separated trailing edge area. Once the DTWs reach the trailing edge, UTWs are created in order to respect the Kutta condition. Hartmann et al. (2013) stated that the UTWs start reaching the shock in the last part of the downstream movement, forcing the shock

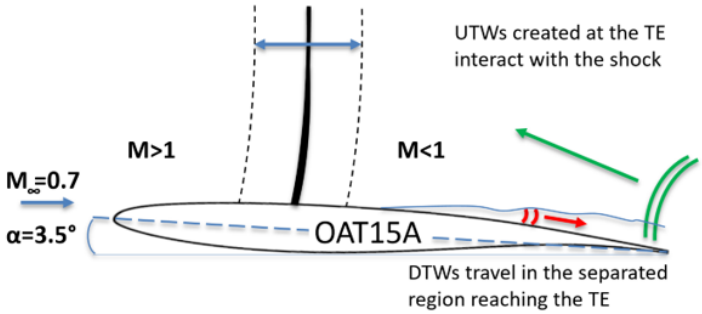

Figure 1: Sketch of transonic buffet feedback mechanism

to start moving upstream. During the upstream movement, the widened area of separated flow reduces the formation of DTWs and, consequently, of UTWs, therefore the shock upstream movement is not sustained by the UTWs' energy anymore and so stops its upstream movement, closing the feedback mechanism. In this description it is still not clear from literature if the UTWs are created only during part of the cycle or during the whole cycle but with a modulated strength.
A different explanation of buffet is given by Crouch et al. (2009), who described it as a consequence of global instabilities present in the flow. These results are in good agreement with those previously reported, therefore, the feedback outlined can be seen as the physical mechanism of these global instabilities.

2 Experimental procedures

An experimental investigation of the role of UTWs in the buffet cycle has been carried out in the transonic-supersonic wind tunnel (TST-27) of Delft University of Technology which is a blowdown wind tunnel with a test section 270 mm high and 280 mm wide.
The model used is the supercritical airfoil, OAT15A with a chord of 100 mm and a span of 200 mm. This airfoil has been designed by ONERA and it has been chosen because of its wide use in the studies on transonic buffet both in experimental (Jacquin et al. (2009)) and numerical studies (Deck (2005)). In contrast to previous experiments that have been performed in the same wind tunnel (Schrijer et al. (2018), D'Aguanno et al. (2019)) the airfoil has been oriented vertically in the wind tunnel, mounting it to pylons that are connected to the vertical side wall of the tunnel, as shown in Fig. 2(a) and Fig. 3(a) . This configuration offers an optimal optical access to the suction side of the airfoil, in order to study the spanwise organization of the UTWs, while also providing the possibility to change the angle of attack. In order to ensure a turbulent boundary layer, a transition trip has also been applied at 7% of the chord.
To investigate the flow field two optical techniques were used: Background Oriented Schlieren (BOS) to investigate the (unsteady) wave pattern and Particle Image Velocimetry (PIV) to capture the instantaneous velocity field.
To apply the BOS technique, the surface of the airfoil was covered with a speckle pattern foil as shown

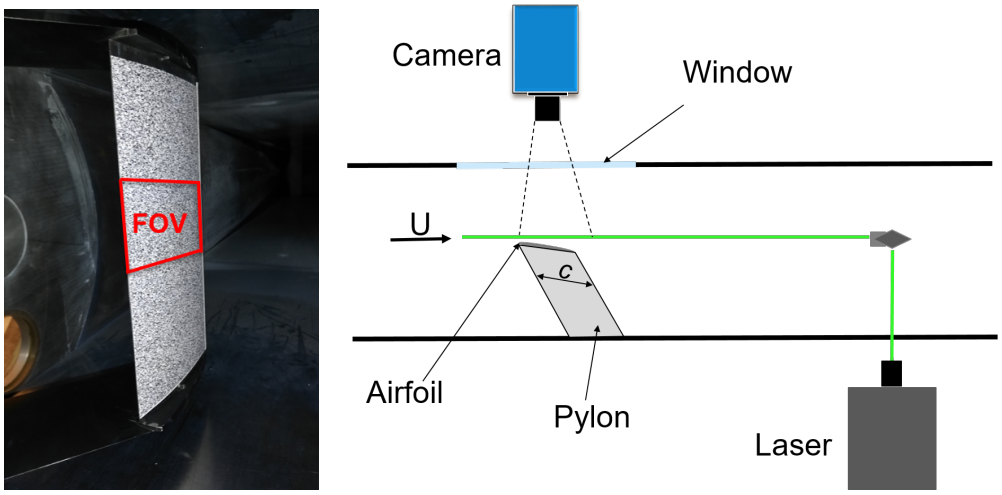

(a) Airfoil with speckle pattern (b) PIV set-up (top view)

Figure 2: Experimental set-up for BOS and PIV

in Fig. 2(a). Here the rectangular area indicates the Field of View (FOV) of interest, which ranges from 15% to 100% of the chord in the chordwise direction and from -30% to 30% of the chord in the spanwise direction (relative to the mid span location). In order to observe and track the speckle pattern movement in time, a high speed camera (Photron Fastcam SA1.1.) was used together with an LED continuous lamp. The frequency of the camera is 5 kHz, which is sufficient to resolve the shock oscillation in time which has a typical frequency of 160 Hz.
The images have been acquired using the camera software PFV (Photron Fastcam Viewer) with a resolution of 1024*640 pixel, a 105 mm lens , a f-stop of 2.8 and an exposure time of 15 μs. The images have been

processed using Davis 8.4.0. Two types of processing have been carried out. The first is a standard procedure in which each BOS image is correlated with a reference image obtained with the wind tunnel off. The second takes a differential approach by correlating each consecutive image with the following. In both cases a multi-pass approach has been chosen for the correlation, using two initial passes with a window size of 64*64 pixels and two subsequent passes with a window size of 24*24 pixels and an overlap of 75%.
In Fig. 2(b) the set-up of the PIV experiment is shown. In this case too, a Photron Fastcam SA1.1 camera was used, operated in double pulse mode (Δt=3μs), with an acquisition frequency of 4.65 kHz and a resolution of 1024*640 pixels. The PIV images were obtained by seeding the flow with DEHS particles and illuminating them with a Mesa PIV dual-cavity high-speed Nd:YAG laser. The laser sheet is parallel to the vertical side walls of the wind tunnel and therefore in the direction of the flow. As displayed in Fig. 3(b), the area illuminated by the laser is at a non-constant distance from the surface of the airfoil, the laser sheet was located at a distance of 1 mm from the airfoil in correspondence to its thickest point and at a distance of 10 mm from the surface at the trailing edge. The projection of the FOV on the airfoil is silmilar to BOS and ranges from 15% of the chord to the trailing edge.
For the PIV measurements, the data were acquired and processed in Davis 8.4.0. Since the raw images were affected by reflections caused by the proximity of the airfoil surface to the laser sheet, first, a minimum subtraction using a Butterworth filter was applied, followed by a cross-correlation procedure to obtain the 2D velocity field. As in BOS, the cross correlation is computed with a multi-pass approach with 2 passes of 64*64 pixels and 2 passes with a final window size of 24*24 pixels; in both cases an overlap of 75% has been chosen, resulting in a vector spacing of 0.5% of the chord.

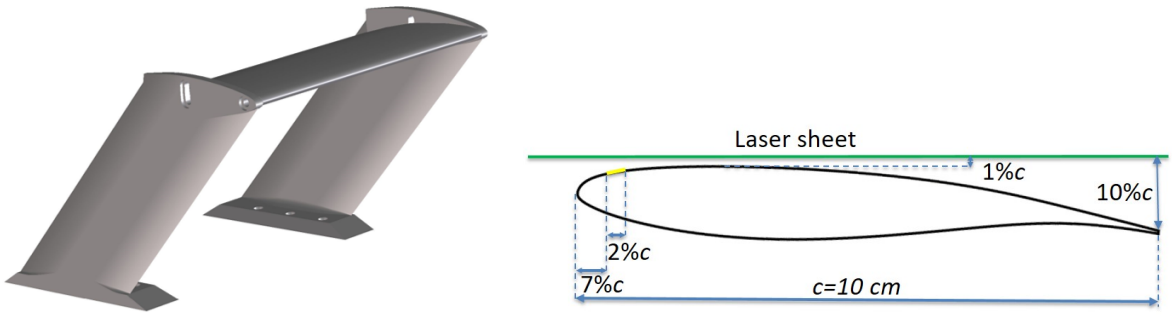

(a) Airfoil mounted on its pylons

(b) Laser sheet position

Figure 3: OAT15A airfoil

3 Results

In this section, first results obtained with BOS will be analysed, and after those obtained with PIV. It is worthwhile to note that all the outcomes discussed are for a Reynolds number relative to the chord $Re = 2 \cdot 10^6$, for an angle of attack α=3.5, and nominal $Ma = 0.7$ (blockage corrected value $Ma_{corr} = 0.73$). These conditions have been selected since previous experiments (Schrijer et al. (2018)), show that shock buffet is fully developed.

3.1 BOS

From the BOS results it is possible to have both a qualitative and a quantitative description of the shock buffet mechanism. In Fig. 4(a) a typical BOS instantaneous processed image is shown displaying the displacement map of the speckle pattern, highlighting two of the main elements of buffet: the shock wave and two UTWs that move from the trailing edge towards the shock position. This image has been obtained using the "normal" procedure by correlating the deformed image of the speckle pattern with the no-flow reference image, so in this image the displacement map of the speckle pattern in the flow direction is portrayed.
Instead, Fig. 4(b) shows, for the same time instant, the BOS image obtained with a differential processing where two consecutive raw images have been processed. This procedure is similar to the one that has been referred as "monoscopic BOS" in literature and it is described in more detail by Bauknecht et al. (2014) and

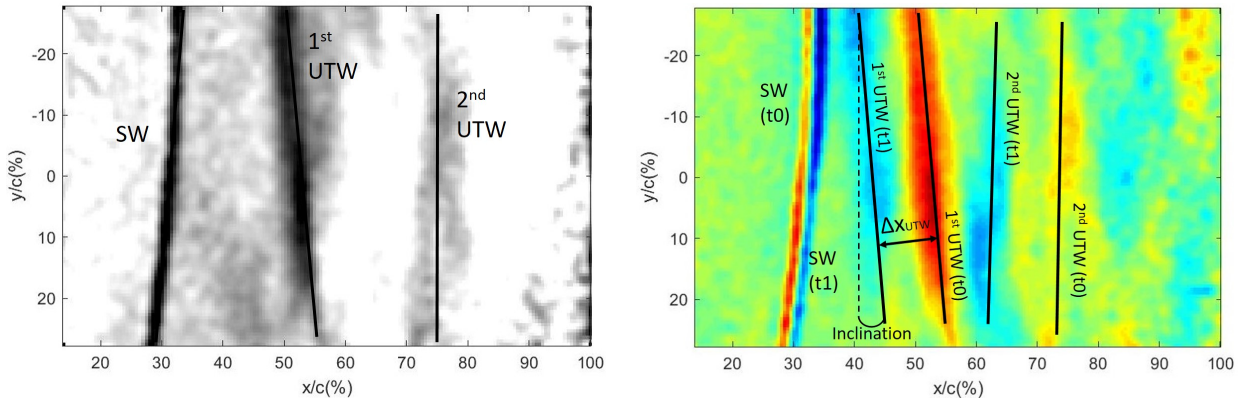

(a) "Normal" BOS image (b) "Monoscopic" BOS image

Figure 4: BOS instantaneous images

Raffel (2015).
Fig. 4(b) shows the relative displacement of the speckle pattern between the two images, hence the processed image results in the presence of both the shock at time t_0 (in red) and the shock at the following time step ($t_1 = t_0 + 0.0002s$) (in blue), therefore,the two shock waves appear with an opposite sign in the displacement map. The distance between these two patterns represents the displacement of the shock between the two time frames. Similarly, even the UTWs observed at both the time steps appear in the same image (in red the UTWs belonging to the first one and in blue to the second one). It is worthwhile to consider that this differential method can be used only for applications in which the density gradient is moving relative to the field of view and the time between two consecutive images is big enough in order not to have overlapping density gradients belonging to the two different time steps; for this research both these conditions are met.
Thanks to the high density of information, each image indicates whether the shock is moving upstream or downstream (downstream in Fig. 4(b)), while the distance together with the time separation allows the computation of the velocity of the shock wave and of the UTWs. In Fig. 4(b) the distance Δx_{UTW} indicates the space covered by the first UTW in one time step and this displacement is considered orthogonal to the front of the wave.
By storing the shock position in time for each instantaneous image, it has been possible to construct the

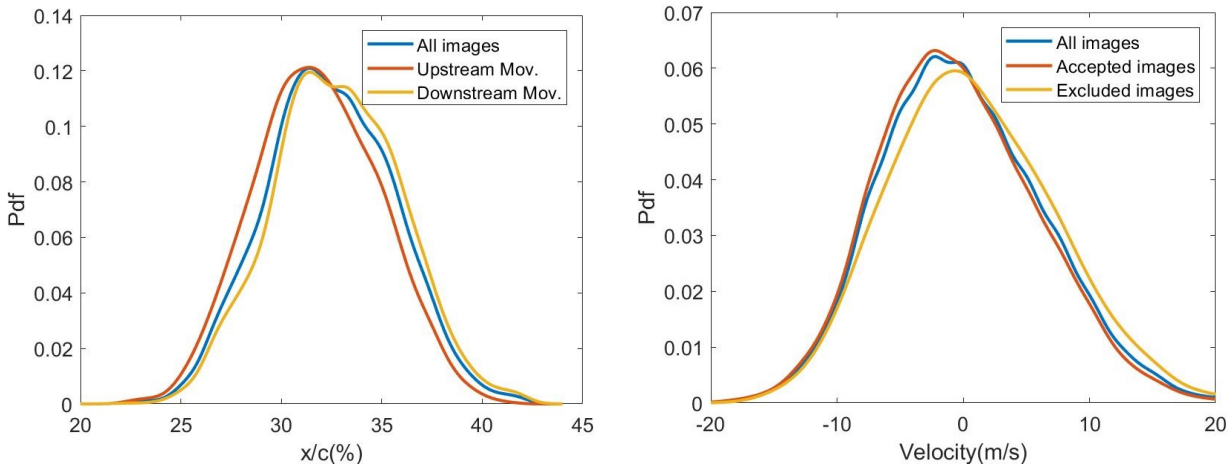

(a) Pdf of the shock position (b) Pdf of the shock velocity

Figure 5: Pdf of shock wave

probability density function (Pdf) of finding the shock in a certain position. In particular, Fig. 5(a) shows that the region in which the shock is most likely to be found ranges from 25 to 40% of the chord. Depending

on the shock movement (upstream or downstream), the BOS images have been divided into two additional groups and Fig. 5(a) demonstrates that, though there being no important variation in the shock position during the two phases, slightly more upstream positions are present during the upstream movement.
From the information of the shock position in time obtained from the "Normal BOS" images, the shock velocity has been computed and Fig. 5(b) shows that the velocity of the shock wave ranges from -18 to 20 m/s, therefore being more probable to have slightly higher velocity during the upstream movement (positive velocities) compared to the downstream movement (negative velocities).
A subsequent spectral analysis has been performed to evaluate the amount of energy associated to the shock oscillation. In order to do this, the pre-multiplied power spectral density associated to the shock position has been computed with the Welch method and plotted in Fig. 6. It is evident from this plot (blue line)

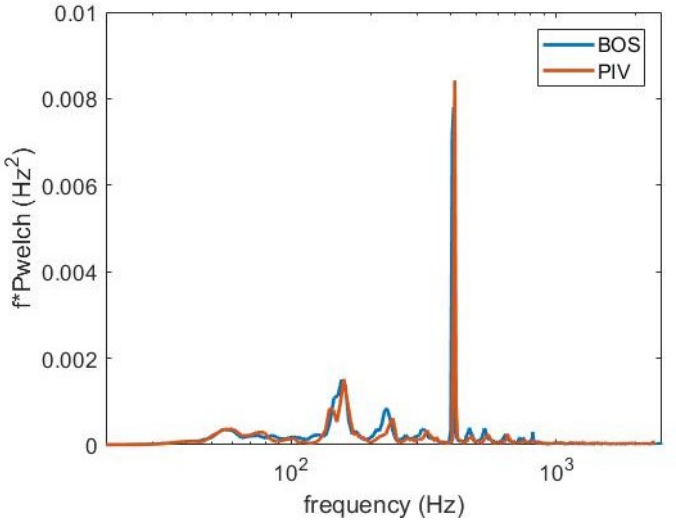

Figure 6: Psd of the shock position for BOS and PIV data

that the main contributions to the shock oscillation are at 160 Hz and 400 Hz. The peak at 160 Hz is the typical one related with buffet, consistent with Schrijer et al. (2018); this frequency is associated with a non-dimensional Strouhal number St=0.067 that is identical to the one obtained for the same airfoil in other experiments present in literature (Jacquin et al. (2009)). On the other hand, the main peak present at 400 Hz is associated to a characteristic frequency of the wind tunnel, which is particularly evident for this experimental configuration.

3.1.1 Autocorrelation analysis

In order to reliably detect the UTWs an autocorrelation analysis of the "Differential BOS" images was performed. To understand whether the emission of UTWs is associated with just one of the two main phases of the shock oscillation, the upstream and the downstream phases of the shock oscillation are treated separately. The region in which the autocorrelation is evaluated goes from 40% to 95% of the chord in the chordwise direction, while it goes from -20% to +20% of the chord in the spanwise direction (always in relation to the mid-span location). In Fig. 7 the instantaneous autocorrelation map corresponding to the BOS processed image of Fig. 4(b) is given. At the centre of the autocorrelation map, in red, there is the main peak corresponding to the point ($\Delta x = 0mm, \Delta y = 0mm$). Both at the right and at the left of this peak, two negative peaks can be observed. These peaks are due to the presence of the same UTW, but at different time instances and being the density gradients associated to the same UTW at different time steps of different sign, the corresponding peak in the autocorrelation map appears negative. Hence, the distance between the positive and negative main peak gives an indication of the distance covered by the UTWs in the time between two consecutive images (Δt=200 ms). The secondary positive peak present in the autocorrelation map ($\Delta x = -20mm, \Delta y = 0mm$) is instead associated with the presence of the second UTW that is observable in the BOS image.
Fig. 4(b) clearly shows the presence of both the first and the second UTW, but unfortunately this is not the case for all images. In order to obtain proper averaged statistics, not affected by these images, a procedure

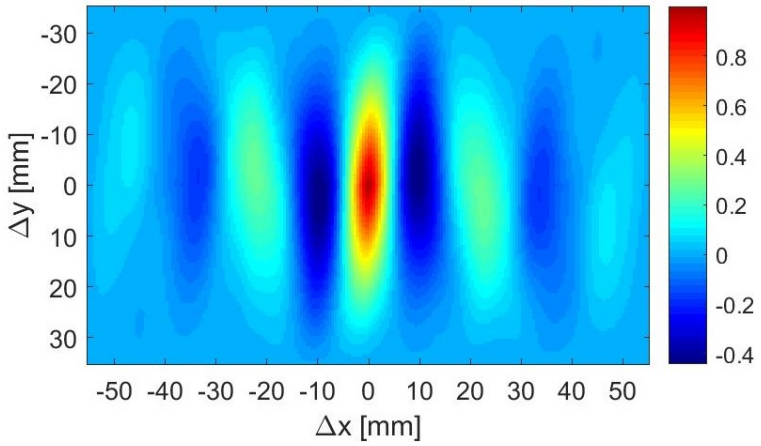

Figure 7: Instantaneous autocorrelation map

for rejecting images when no clear UTW was detectable is applied. This information could furthermore be used to monitor if those images were rejected in a specific phase, thus suggesting that the production of the UTWs happens in a specific phase of the buffet cycle. To show this point, in Fig. 5(b) the distribution of the velocity of the shock wave is plotted in presence of all the images (8000 images), in absence of the rejected images (5281 images) and just for the rejected ones (2719 images). This plot clarifies that the distribution of the velocity profile remains unchanged for these three groups of images, suggesting that the images in which no clear UTWs have been detected do not belong to a specific phase of the buffet cycle.
The instantaneous correlation maps are used to find the inclination and the velocity of the UTWs at each

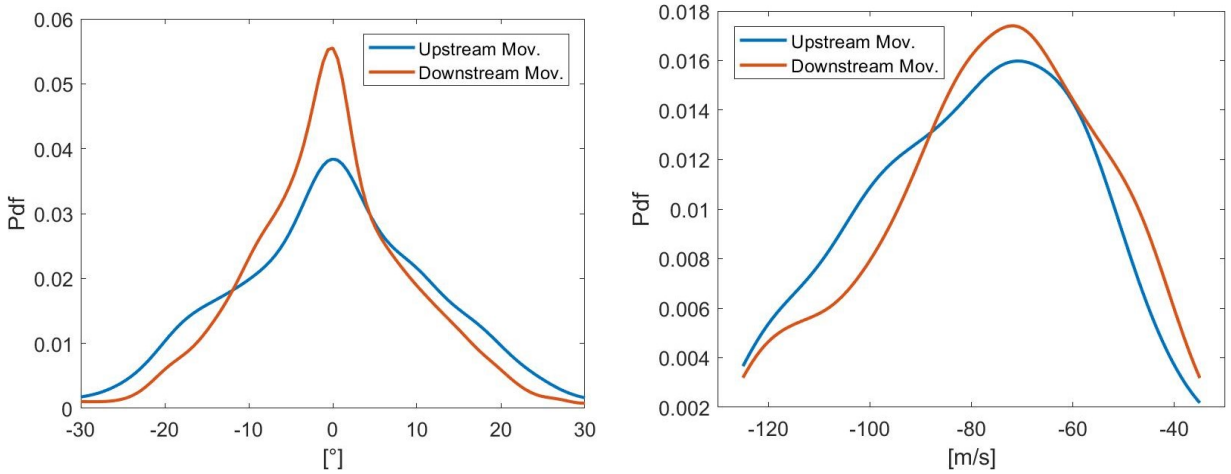

(a) Pdf of the inclination of the UTWs

(b) Pdf of the velocity of the UTWs

Figure 8: Pdf of UTWs

time step. From these maps it is clear that the UTWs propagate in the flow with a certain inclination that ranges from negative to positive angles (as shown in Fig. 4(b)). By detecting the angle of the UTWs for each instant it was possible to evaluate both the mean value and the probability density function of its distribution both for the upstream and the downstream phase of the buffet cycle, as shown in Fig. 8(a). First of all it is interesting to notice that the mean value of the inclination is zero for both the phase of downstream and upstream movement. Despite the values of inclination ranging from -25 to +25 degrees in both phases, during the upstream movement it is more probable to have higher angles of inclination, therefore, the peak of the probability density function at small angles of inclination is much higher during the downstream movement. However, from a spectral analysis of the inclination in time, no clear peak is observable, suggesting that the variation of the inclination in time does not actually depend on the buffet phases, therefore, this information

is not shown here.
From each instantaneous autocorrelation map, the velocity of the UTW has been evaluated by looking at the distance between the positive and negative peak of the map and plotted in Fig. 8(b) in terms of Pdf. The average velocity obtained is 78.1 m/s during the upstream travel and 74.9 m/s for the downstream one, values which are close to the ones obtained by Hartmann et al. (2013) (80 m/s). But differently from what is shown in this previous study, the Pdf of the UTW velocity shows that there is a range of velocities for the UTWs that varies from -125 to -35 m/s. This range of velocity can be justified by the assumption that the UTWs, behaving like pressure waves, travel at the speed of sound relative to the flow. There is a difference in the velocity of the UTWs obtained during the upstream and downstream movement of the shock, having a distribution of velocity moved to higher velocities during the upstream movement (in terms of absolute values). This result is explained, by considering that during the upstream movement of the shock, the separated area is wider and the flow velocity near the airfoil surface lower, therefore, higher velocities for the UTWs are expected.
Averaging the instantaneous autocorrelation maps an average map has been obtained, both for the upstream and the downstream movement. In Fig. 9(a) the average autocorrelation map for the downstream movement is shown. Also in this map it is possible to observe the presence of a positive main peak at the centre, a negative one and a second positive peak, similar to the instantaneous map. Since the velocity of the UTWs changes in time, both the secondary positive peak and the negative peak are located in slightly different locations in time, therefore the peaks in the average correlation map are less defined than those in the instantaneous correlation map. Comparing this data to the instantaneous one in Fig. 7, it is even possible to see that other secondary peaks are not present in the average map, since in most of the images the signal to noise ratio related to these peaks is too low.
In order to compare the results for the upstream and downstream movement, the values for the average autocorrelation map obtained for $\Delta y = 0$ are presented in Fig. 9(b). Even in this plot no important differences are present between both phases, meaning that the propagation of the UTWs occurs to a similar extent during these two phases. However, during the downstream movement the value of the negative peak and of the second positive peak, in the correlation map, is slightly reduced compared to the upstream case, leaving the possibility of the modulation of the strength of the UTWs along the buffet cycle still open.
From the average autocorrelation map, looking at the distance between the two positive peaks (which represents the average spacing between subsequent waves), the average frequency with which the UTWs are produced has been obtained (considering as propagation velocity the average one). This frequency is equal to 2300 Hz and corresponds to a Strouhal number of 0.96, which is in good agreement with the value reported by Hartmann et al. (2013).

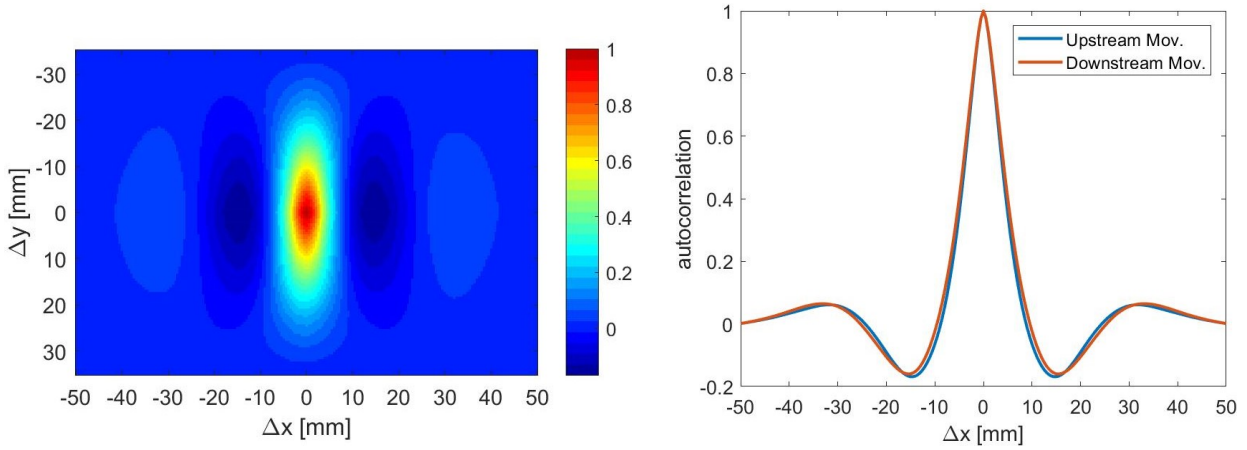

(a) Average autocorrelation map for downstream movement

(b) Profile of autocorrelation map

Figure 9: Autocorrelation during the upstream and downstream movement of the shock

3.2 PIV

The PIV results are discussed to corroborate those obtained with BOS and to quantify the velocity field. First the instantaneous PIV images are inspected, showing the main structure of the flow field. In Figs. 10(a), 10(b) the horizontal component of the velocity field (in the free stream direction) is shown for two instantaneous consecutive PIV images, with a time interval of 0.22 ms. These velocity fields also allow the detection of the presence of a shock wave, an UTW and the separated flow area, the latter characterized by the low velocity region towards the trailing edge of the airfoil. It is worthwhile to mention once again that in this case the plane of measurement is not at a constant distance from the airfoil, as previously shown in Fig. 3(b), therefore, this configuration cannot determine the size of the separated area accurately. In these plots the shock wave is moving upstream, while the UTW at first emerges from the separated area and then moves towards the shock location. Here too, the UTW is travelling upstream with a non zero inclination, although as for BOS, it has a zero mean value in time. Notwithstanding the inclination of the UTW, it is possible to see how the background flow field is nominally 2D, without changes in velocity in the spanwise direction both in the supersonic and subsonic region, including the separated area.
For PIV, the detection of the shock location for each image is based on the velocity gradient; Subsequently,

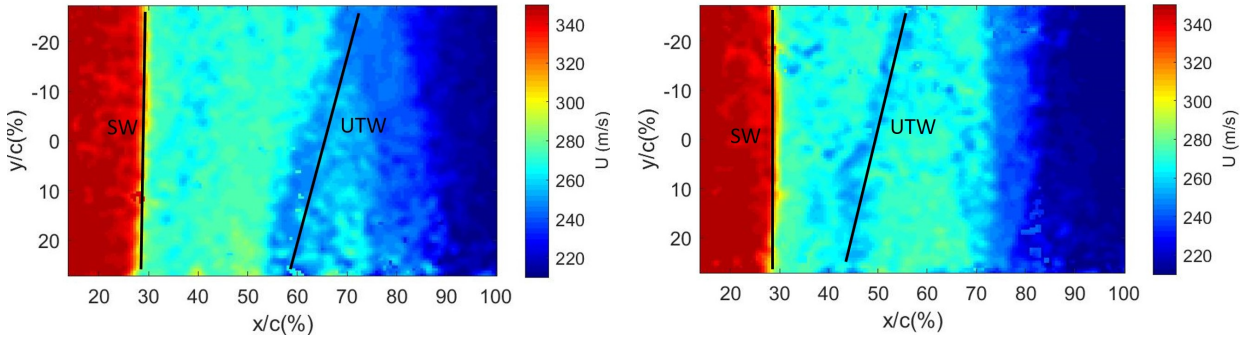

(a) Velocity field (U) at time t_0

(b) Velocity field (U) at time $t_1 = t_0 + 0.22ms$

Figure 10: Instantaneous PIV images

from the spectral analysis of the shock position in time, the power spectral density associated to it has been evaluated. In Fig. 6 the pre-multiplied power spectral density is displayed both for PIV and BOS, showing a very good agreement between the two techniques. In both cases it is possible to identify the presence of the classic buffet peak at 160 Hz (St=0.067) together with a strong additional peak at 400 Hz that is associated with the noise in the wind tunnel.

3.2.1 Triple decomposition of the velocity field

As buffet is an unsteady quasi-periodic phenomenon, it is convenient to express the velocity field using the so called triple decomposition:

$$u = u_{Avg} + u_{Phs} + u_{Turb} \tag{1}$$

in which u_{avg} is the mean component of the velocity, while u_{phs} a periodic one and finally u_{turb} a quasi-random fluctuating component. The periodic component is obtained by dividing the PIV processed images into eight different groups, depending on the shock position and direction of movement. The first phase indicates the phase in which the shock is in its most upstream position, while the fifth phase in its most downstream position, a more detailed description of the buffet phases is given in D'Aguanno et al. (2019). In Fig. 11(a), 11(b) the phase averaged velocity field for the U component is shown, for reason of brevity, just for the most downstream (left) and upstream (right) position. These velocity fields demonstrate that the distance between the shock position in the most downstream and upstream position is 5% of the chord, therefore, the amplitude of the shock oscillation is smaller for this configuration compared to other experiments present in literature for the same airfoil. However, it should be noted that being the amplitude of the shock oscillation not constant for each cycle, slightly different positions are averaged when evaluating the average of the flow field for each phase, bringing to a smoother reduction of velocity in correspondence of the shock. This data still confirms that buffet on a 2D airfoil behaves as a 2D problem in terms of average

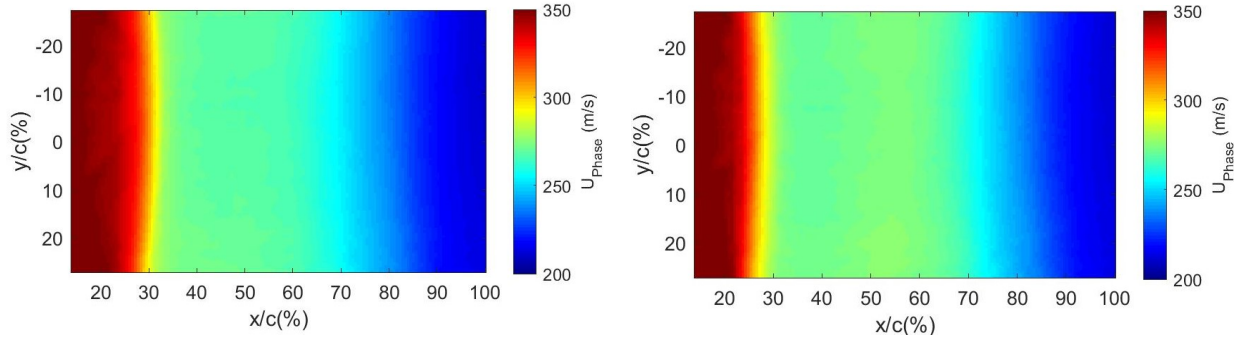

(a) Velocity field in the most downstream position

(b) Velocity field in the most upstream position

Figure 11: Phase averaged velocity in the most upstream and downstream position

flow field, not having important differences in the spanwise direction (both for the shock wave and for the separated area), at least far away from the wing tips.

3.2.2 Estimated upstream travelling waves velocity

A detailed evaluation of the UTW velocity of the PIV images is more complex than for the BOS images, since in the former case it is not always possible to correctly detect the UTWs because of the separated area. However, starting from the PIV images it has been possible to verify whether the range of velocity of the UTWs obtained with the BOS technique is the expected one and so confirm whether the UTWs really propagate at the velocity of sound in relation to the flow. Under this assumption the local velocity of the UTWs is expressed as the difference between the local velocity and the local speed of sound:

$$U_{UTWs} = U_{loc} - a_{loc} \tag{2}$$

Assuming the adiabatic flow of an ideal gas, the local speed of sound can be expressed in terms of the local total velocity (V):

$$a = \sqrt{\gamma RT} = \sqrt{\gamma R(T_0 - \frac{V^2}{2c_p})} \tag{3}$$

Starting from the average velocity field, the expected range of velocity for the UTWs is shown in Fig. 12(a) on the right. The rectangular area indicates the area in which the autocorrelation analysis for BOS was computed; in this area the difference between the local velocity and the speed of sound ranges between -100 and -50 m/s and therefore agrees with the range of the computed velocity for the UTWs. Applying the same procedure to all the instantaneous images, the probability density function of the estimated UTWs' velocity has been acquired and plotted in Fig. 12(b). The range of the velocity obtained matches the BOS experimental results very well as shown with the dashed line in the plot. This result confirms the acoustic nature of the UTWs which propagate in the flow field with the speed of sound.
However, it should be noted that the average velocity for the UTWs, estimated with this procedure, is around 70 m/s (in absolute value), which is almost 10 m/s lower than the one obtained with BOS. This discrepancy could be attributed to the fact that the average velocity values obtained with PIV are slightly higher than those close to the surface of the airfoil, since the measurement plane is less influenced by the presence of a separated area, hence overestimating the effective downstream flow velocity which results in a reduction of the UTW velocity. This result is confirmed in Fig. 12(b), by observing that both the estimated velocity ranges for the UTWs (for upstream and downstream movement) are moved to the right compared to the BOS results. The bigger discrepancy is present for high velocities (in absolute value), which as described previously are reached near the trailing edge area. In Fig. 12(b), just negligible differences between the upstream and downstream movement are observed for the PIV measurements.

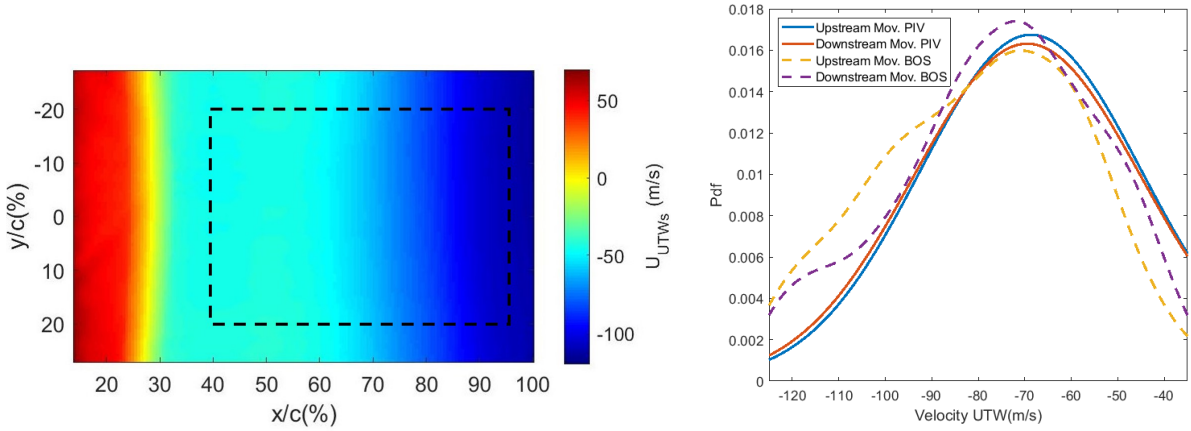

(a) Estimated average velocity of UTWs

(b) Pdf of the velocity of the UTWs

Figure 12: Velocity range of the UTWs

4 Conclusion

In this paper a study on the importance of the upstream travelling waves in transonic buffet has been reported and both BOS and PIV have demonstrated to be suitable techniques for this research. In particular, the use of the differential BOS has facilitated the detection of the UTWs and their propagation velocity. It has been clarified that the velocity of propagation of the UTWs is not constant, but is equal to the speed of sound in relation to the flow, as corroborated with the PIV data, and ranges from -120 to -40 m/s. An average propagation frequency of the UTWs of 2300 Hz has been computed, which is in good agreement in terms of Strouhal number with Jacquin et al. (2009) and Hartmann et al. (2013).
It was demonstrated that although the average inclination of the UTWs is near zero, they display a non zero instantaneous angle of inclination, without important differences between the statistics for the upstream and downstream phases of the buffet cycle. Despite this, the specific set-up revealed, once again, the coherence of the shock wave and of the separated area in the spanwise direction.
It is worthwhile to consider that the results have been obtained processing the original data directly without applying any filtering procedure.
The subdivision of the buffet cycle in the upstream and downstream shock movement phases has confirmed that the UTWs are produced throughout the entire buffet cycle and the images in which no clear UTW is detected do not belong to a specific buffet phase. However, small differences present between the upstream and the downstream movement suggest the possibility of a modulation of the strength of the UTWs during the buffet cycle. Therefore, it is expected that the stronger UTWs will be produced when the shock is approaching the most downstream position, forcing it to stop its travel and start its upstream movement. Strong UTWs will still be present in the first part of the upstream movement and together with a separated growing area will sustain its movement. After this the shock wave will still interact with UTWs, but with reduced strength and a reduction of the separated area too, the shock will stop its upstream travel, closing the feedback mechanism. To conclude, even if promising results have been obtained, in order to fully comprehend the problem, a deeper understanding of the mechanism by which the strength of the UTWs is modulated is required.

References

Bauknecht A, B Merz C, Raffel M, Landolt A, and Meier A (2014) Blade-Tip Vortex Detection in Maneuvering Flight Using the Background-Oriented Schlieren Technique. *Journal of Aircraft* 51(6):2005-2014

Crouch JD, Garbaruk A, Magidov D, and Jacquin L (2009) Global structure of buffeting flow on transonic airfoils. in *IUTAM Symposium on Unsteady Separated Flows and their Control*. pages 297–306

D'Aguanno A, Schrijer F, and van Oudheusden B (2019) Transonic Buffet Control by means of Upper Gurney Flaps. in *Proceedings of the 54th International Conference on Applied Aerodynamics (3AF 2019)*

Deck S (2005) Numerical simulation of transonic buffet over a supercritical airfoil. *AIAA Journal* 43:1556–1566

Garnier E and Deck S (2010) Large-eddy simulation of transonic buffet over a supercritical airfoil. in V Armenio, B Geurts, and J Fröhlich, editors, *Direct and Large-Eddy Simulation VII*. pages 549–554. Springer Netherlands, Dordrecht

Hartmann A, Feldhusen A, and Schröder W (2013) On the interaction of shock waves and sound waves in transonic buffet flow. *Physics of Fluids* 25(2):026101

Hilton WF and Fowler RG (1952) Photographs of shock wave movement. ARC R&M 2692

Jacquin L, Molton P, Deck S, Maury B, and Soulevant D (2009) Experimental study of shock oscillation over a transonic supercritical profile. *AIAA Journal* 47:1985–1994

Lee BHK (1990) Transonic buffet on a supercritical aerofoil. *The Aeronautical Journal* 94(935):143-152

Raffel M (2015) Background-oriented schlieren (BOS) techniques. *Experiments in Fluids* 56:60

Schrijer F, Solana Perez R, and van Oudheusden B (2018) Investigation of transonic buffet using high speed PIV. in *Proceedings of the 5th International Conference on Experimental Fluid Mechanics (ICEFM 2018)*